nature geoscience

ARTICLES

PUBLISHED ONLINE: 5 JANUARY 2015 | DOI: 10.1038/NGEO2335

Complexity of the deep San Andreas Fault zone defined by cascading tremor

David R. Shelly

Weak seismic vibrations—tectonic tremor—can be used to delineate some plate boundary faults. Tremor on the deep San Andreas Fault, located at the boundary between the Pacific and North American plates, is thought to be a passive indicator of slow fault slip. San Andreas Fault tremor migrates at up to 30 m s^{-1}, but the processes regulating tremor migration are unclear. Here I use a 12-year catalogue of more than 850,000 low-frequency earthquakes to systematically analyse the high-speed migration of tremor along the San Andreas Fault. I find that tremor migrates most effectively through regions of greatest tremor production and does not propagate through regions with gaps in tremor production. I interpret the rapid tremor migration as a self-regulating cascade of seismic ruptures along the fault, which implies that tremor may be an active, rather than passive participant in the slip propagation. I also identify an isolated group of tremor sources that are offset eastwards beneath the San Andreas Fault, possibly indicative of the interface between the Monterey Microplate, a hypothesized remnant of the subducted Farallon Plate, and the North American Plate. These observations illustrate a possible link between the central San Andreas Fault and tremor-producing subduction zones.

The relationship among tremor, low-frequency earthquakes (LFEs) and slow slip has fuelled vigorous scientific debate over the past decade. A growing consensus agrees that larger-scale slow slip typically drives failure on numerous smaller asperities that slip more suddenly[1]. These more sudden events are rapid enough to generate seismic waves at frequencies of 2–8 Hz (and often higher), although they are depleted in higher frequencies relative to typical earthquakes. Individually, these events are LFEs, but in most cases multiple LFEs occur in rapid succession, generating a semi-continuous signal referred to as tremor[2]. Here, I use 'LFEs' to refer to individual events and 'tremor' to refer to the phenomenon more broadly, but otherwise I consider the terms interchangeable.

Tremor source propagation occurs at multiple velocities and spatial scales. At the slow end, tremor propagates at ∼10 km d^{-1} along strike in the Nankai[3] and Cascadia subduction zones, where in the latter it sometimes continues for more than 200 km (ref. 4). Faster migration, at ∼30–150 km h^{-1}, was first observed in Nankai[2,5], with similar behaviour also seen in Cascadia[6] and along the strike-slip San Andreas Fault[7]. This high-speed migration seems to occur in the orientation of relative plate motion[6], which is roughly the dip direction for subduction zones but along strike for the San Andreas. Recently, tremor propagation with intermediate velocities (7–17 km h^{-1}) has also been observed, termed 'rapid tremor reversal' events because they propagate primarily backwards from the direction of overall slow slip propagation[8]. Multiple mechanisms have been put forth to explain the varied migration behaviours, such as large-scale fluid flow[6], interaction of slow propagation with slip-aligned heterogeneity[9,10], or a two-state-variable friction law[11]. A consensus has yet to emerge, however, underlining fundamental gaps in our understanding of slow slip and tremor phenomena.

In this paper, I explore overall migration characteristics between pairs of San Andreas tremor sources by generating a 12-year time series for each source location and cross-correlating all possible time series pairs (see Fig. 1 and Methods). This approach circumvents some of the complexity inherent in identifying individual migration episodes[12,13]. I focus on high-speed migration, with time lags between sources of up to two hours, and explore the implications for the underlying source physics and structure of the fault zone.

Tremor migration patterns

Figure 2 shows LFE family pair correlations within lags of ±2 h. These correlations demonstrate how commonly activity in each family is preceded or followed by activity in neighbouring families within this time window. The area of strongest interfamily correlations is the zone southeast of Parkfield beneath Cholame (10–40 km along-strike position), a zone that also hosts the strongest tremor observed in the area[14,15]. In this zone, correlations are detected up to a separation distance of ∼20 km along strike (Fig. 3a and Supplementary Fig. 1). Relatively strong correlations are also observed between families northwest of Parkfield beneath Monarch Peak (−55 to −40 km along-strike position) at up to 15 km distance, a zone that exhibits very strong tidal modulation[16].

The source separation distance is not the only factor controlling these interactions, however. For example, neither of two relatively shallow sources interact with a source only 5 km deeper just southeast of Parkfield (along-strike position ∼3 km). Similarly, relatively shallow sources northwest of Parkfield (along-strike position −25 to −13 km) are only weakly correlated among each other on this timescale, despite their proximity, and these sources are mostly uncorrelated with a group of sources ∼5 km deeper.

Among tremor source pairs that interact (are correlated), I estimate the typical propagation velocity between the sources (Fig. 3). Velocities mostly range from 15 to 90 km h^{-1}. Within this variability, source pairs near the shallower end of the tremor distribution tend to have higher velocities (median 50–60 km h^{-1}) than deeper sources (median velocity 30–40 km h^{-1}), as shown in Fig. 3b, although there is substantial variability. As the depth range of tremor sources varies along strike, I plot velocity as a function of relative depth, measured from the approximate lower limit of tremor at a particular along-strike position (Fig. 2b). Interestingly,

US Geological Survey, 345 Middlefield Road MS910, Menlo Park, California 94025, USA. e-mail: dshelly@usgs.gov

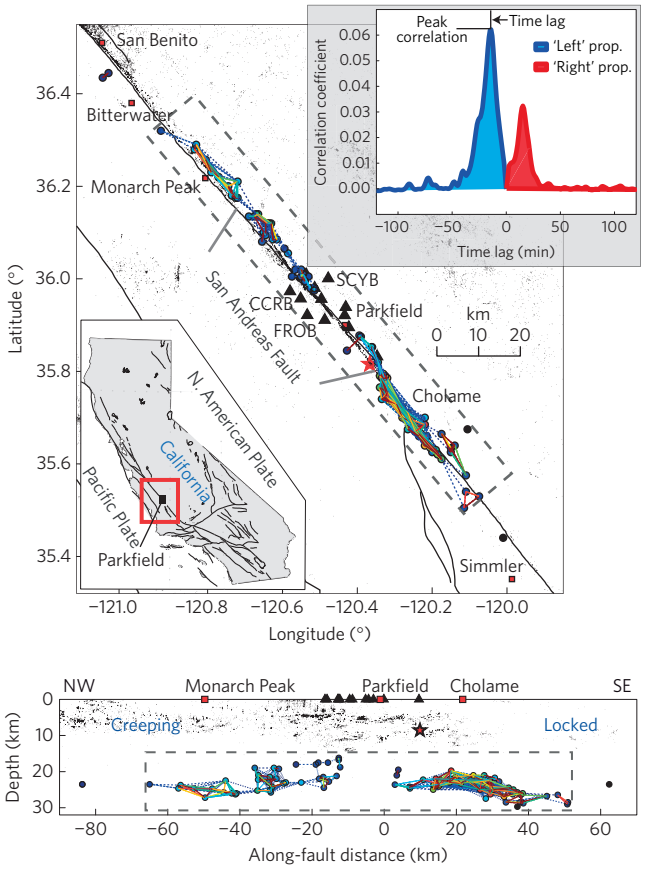

Figure 1 | LFE source family locations[15] along the central San Andreas Fault and their interfamily interactions. Upper panel shows map view; lower panel shows cross-section. Coloured circles are the 88 LFE family locations; coloured lines show interactions. Seismicity (small black dots) is from ref. 39, version v201112.1. Thin black lines are mapped faults. Black triangles are seismic stations used for event detection, including stations SCYB, CCRB and FROB. Dashed rectangles denote regions shown in the zoomed view in Fig. 2. See Fig. 2 for colour scale. Upper right inset shows example correlation function between two families, which reflects the degree of correlation and the typical time lag between activity in these families (Methods). Lower left inset shows the location of Parkfield and map area (red rectangle) in California, with mapped faults.

more energetic LFE families also tend to exhibit higher propagation velocities (Fig. 3c).

Finally, I note that tremor migration is not symmetric—many source pairs exhibit a preferred migration direction, sometimes strongly so (Fig. 2c). In particular, for the zone of tremor southeast of Parkfield, tremor usually propagates from the exterior of this zone along strike towards its centre. The asymmetry may relate to loading patterns of the deep fault. For example, the areas surrounding the tremor zones may slip steadily, loading the edges of the tremor zone, causing propagating slip towards the interior of the zone.

High-speed tremor migration and its regulating mechanism

The high-speed migration velocity, here observed at ~15–90 km h^{-1}, presents a puzzle. This velocity is orders of magnitude faster than the slow, ~10 km d^{-1} along-strike migration of slow slip events, yet also orders of magnitude slower than elastic wave speeds of a few kilometres per second that regulate earthquake rupture velocities. Previously proposed mechanisms such as large-scale fluid flow[6] may be physically implausible, whereas fast migration as simply an apparent velocity of much slower propagation[9] does not seem to explain the patterns of tremor propagation along both strike and dip in Cascadia[17]. Higher propagation velocities kinematically imply higher average slip speeds and/or smaller stress drops[11,17], but the physics underlying this difference remains largely unknown.

As summarized in ref. 11, 'An important question is whether the tremor associated with the secondary fronts [high-speed propagation] is just a passive indicator of increase slip rate... or if it plays an essential role in maintaining that slip.' Although the assumption that tremor is passive is intuitive on the broader scale, with the geodetic moment of slow slip orders of magnitude larger than the cumulative seismic moment of tremor[18], this may not hold true for much smaller-scale, pulse-like rapid tremor propagations (for example, Fig. 4a). Supporting this distinction, tremor propagates most effectively through regions of greatest tremor production (in the case of the San Andreas beneath Cholame), and does not propagate through large gaps in tremor production, such as the gap directly beneath Parkfield (Figs 1 and 2). Likewise, episodes of rapid propagation tend to show continuous tremor/LFE activity, as in the Fig. 4a example. Although this correspondence does not prove that LFE rupture is essential for high-speed propagation, at a minimum it implies that LFE production is encouraged by the same factors that encourage high-speed slip propagation. In either case, some 'braking' mechanism is required to create a seismically stuttering rupture that is stretched out in time relative to a typical earthquake rupture. Furthermore, a plausible mechanism must be applicable in a variety of environments and spatial scales, such that it produces similar behaviour in subduction zones and along the San Andreas Fault.

Recent evidence from laboratory and numerical studies suggests that slip-induced dilatancy may be an important regulating process for tremor and slow slip[19–22]. Slip-induced dilatancy has been proposed to relate to the difference of the logarithms of the slip velocity and initial slip velocity,

$$\Delta\phi_{ss} = \varepsilon \ln\left(\frac{v}{v_0}\right)$$

where $\Delta\phi_{ss}$ is the steady-state change in fault zone porosity (which evolves over a critical slip distance) at sliding velocity v after accelerating from an initial velocity v_0 and ε is the dilatancy coefficient[19,23]. Near-lithostatic fluid pressures, suggested from structural studies of the tremor region in subduction zones[24,25], and from the sense of tidal triggering observed for San Andreas tremor[16,26,27], make dilatant strengthening particularly effective, because the effects of dilatancy are more likely to dominate over frictional and thermal weakening[20].

Slip-induced dilatancy provides a plausible regulating mechanism for high-speed tremor propagation. Assuming that an LFE nucleates as unstable rupture on an asperity embedded in the deep fault, as slip accelerates, the fault zone dilates, reducing the pore pressure, which increases frictional resistance. Figure 4b sketches how this process might unfold. A negative feedback loop is set up because dilatancy is recovered (the fault zone compacts) as slip speed drops again. As slip slows, the combination of resulting compaction and previous fluid inflow allows the fluid pressure to recover, potentially setting up another dynamic slip event. This phenomenon of oscillating slip velocity has been observed in a simple slider-block numerical model[23] from which it was proposed as a possible mechanism for earthquake aftershocks within the mainshock slip region. The same concept has been suggested as a possible mechanism for propagating tremor produced by rerupture of a homogeneous fault[21,22]. However, because the same fault patches consistently generate the strongest tremor[15,28], fault zone heterogeneity (of some type) seems to play an essential role in tremor generation.

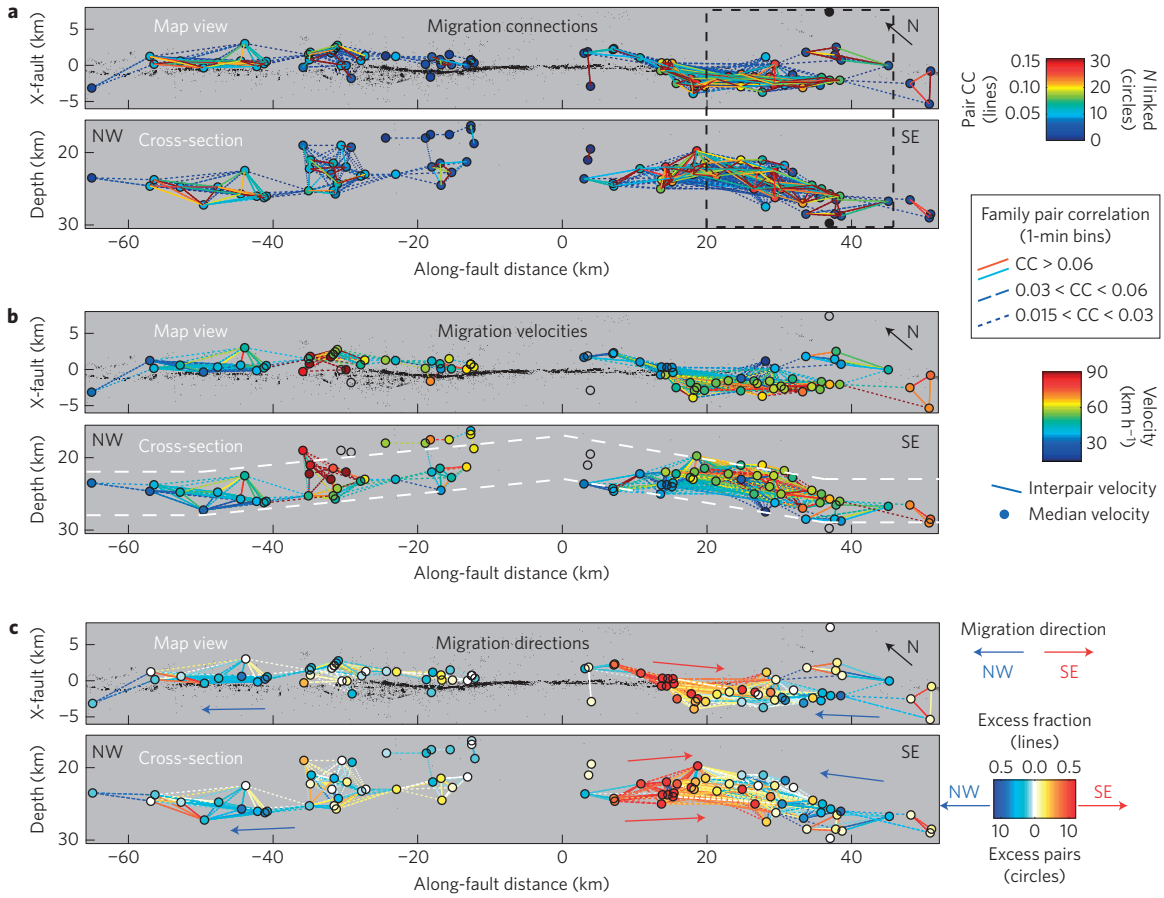

Figure 2 | Migration patterns of LFE families. Shown are rotated map view (upper panels) and along-fault cross-sections (lower panels), as indicated in Fig. 1. **a**, Migration connections among LFE families. Line colours and styles (solid, dashed, dotted) denote the strength of connections, based on the maximum correlation coefficient (CC) between LFE family time series (see legend). Circle colours show the number of connected LFE neighbour families. Small black dots show relocated (upper-crustal) earthquakes[39]. Dashed black rectangle is the area expanded in Fig. 5. **b**, Dominant migration velocities (Methods). Circles are coloured by the median of all connected velocities. Dashed white line denotes zero and −6 km relative depths (Fig. 3b) **c**, Migration direction preference (see Methods and Fig. 1 inset). Solid, dashed and dotted lines in **b** and **c** are the same as in **a**, to help judge robustness.

After the initial rupture, subsequent ruptures are likely to nucleate at stress concentrations near the fringe of the original rupture and expand the overall slip zone, into the adjacent area that has been stressed but not yet ruptured. High along-fault permeability[22] potentially allows rapid fluid pressure diffusion along the fault, although fluid may also diffuse in response to steep gradients in the fault-perpendicular direction. This process could be repeated as long as adjacent fault patches are already very near failure from ongoing surrounding creep. Thus, although this process does not preclude the occurrence of individual LFEs, the static stress transfer could produce a sequence of LFEs propagating along the fault, protracted in time owing to the fluid diffusion time, as in the observed tremor signal (Fig. 4). If fluid flow is primarily confined along the fault, this may introduce an additional scale limitation of slip—as a circular rupture grows, the ratio of rupture area to circumference also grows, and fluid flux across the circumference may be less able to compensate for dilation of the rupture area. I note that this model does not require large-scale redistribution of pore fluid; rather it depends on temporary redistribution of fluid pressure over length scales of individual LFEs (probably tens of metres). Assuming the fault zone is saturated[27], the distance of fluid flow could be much shorter than the scale of fluid pressure change, depending on the volume of slip-induced pore creation relative to the background porosity.

Is this hypothesis realistic? Recent one-dimensional (1D) numerical modelling[22] found that migration speeds ranging from 10 to 150 km h^{-1} could be modelled by assuming certain values of the slip-induced dilatancy rate (α_0) and the permeability (k). In the model, propagation at these speeds required high permeabilities ($>10^{-12}$ m^2) in the fault-parallel direction, compared with permeabilities of 10^{-21}–10^{-13} m^2 estimated for exhumed faults[22]. Although it is unclear whether required permeabilities would be the same in more realistic 2D or 3D geometries, there are several reasons to expect high fault zone permeability. First, nearly lithostatic pore pressures along the deep San Andreas[26,27], should promote high along-fault permeability[29]. Also, ongoing fracturing creates dynamically enhanced permeabilities, which can be orders of magnitude greater than *in situ* permeabilities[30]. Finally, slip-aligned fault corrugations may further enhance along-strike permeability and help focus fluid pressure diffusion along strike.

Faster migration among shallower, more energetic tremor sources could be facilitated by a lower dilatancy coefficient, higher permeability, or a combination[22]. Higher permeability at shallower depth would be consistent with the overall observed trend in permeability with depth in the crust[31] with both propagation velocities and permeabilities subject to substantial local variation. Interestingly, although both LFE family amplitude[15] (recorded ground velocity) and episodicity[32] (recurrence period) correlate with depth, only the amplitude clearly varies with propagation velocity (compare Fig. 3c and Supplementary Fig. 2). The correspondence between tremor amplitude and propagation velocity can also be seen anecdotally in Fig. 4a, where migration

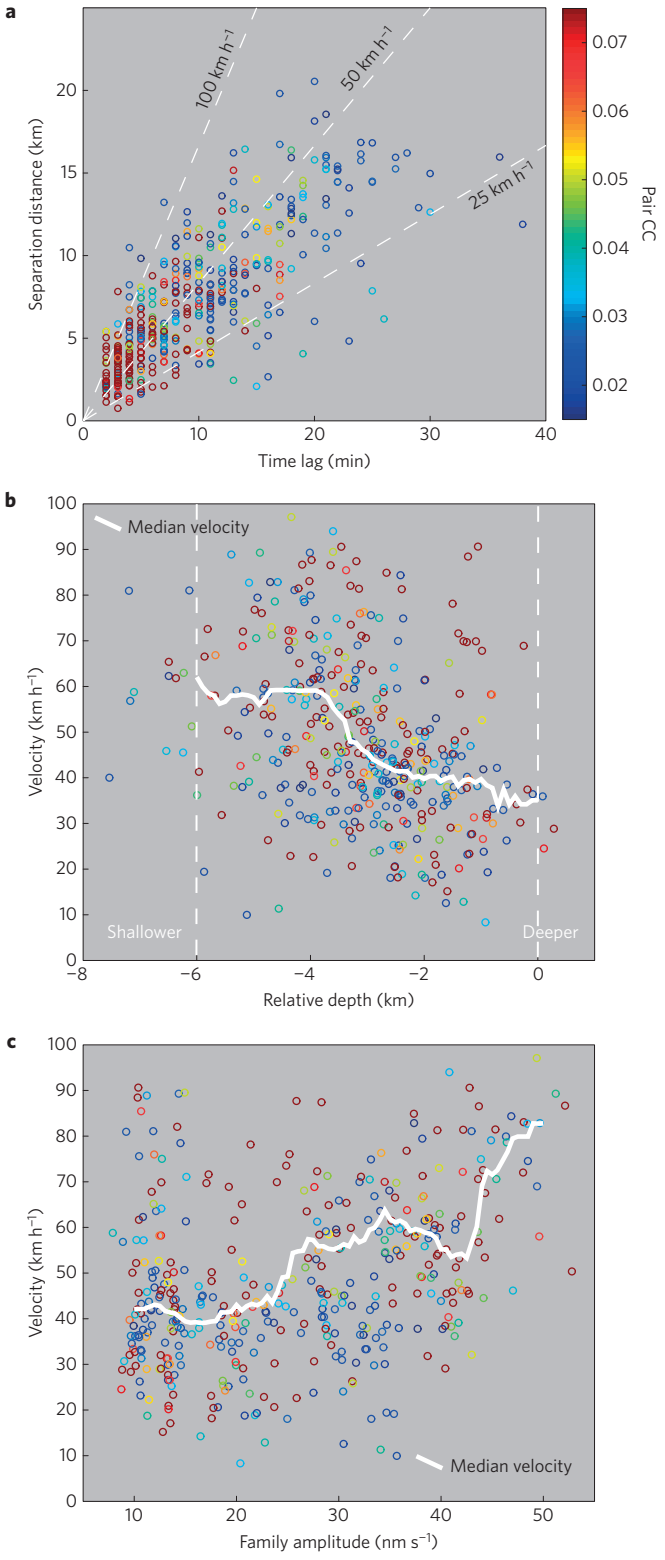

Figure 3 | LFE propagation velocities. a, Separation distance versus lag time for all LFE family pairs correlated above threshold value of 0.015. Circles are coloured by the peak correlation value, with higher correlation values (red) generally representing more reliable measurements. **b**, Velocity as a function of mean relative depth of each LFE family pair. Median velocity is measured using a centred moving window with 1 km width. Relative depth reference lines of zero and −6 km are shown in Fig. 2b. Colour scale as in **a**. **c**, Velocity as a function of LFE family amplitude[15], averaged for each family pair (Methods). Median velocity is measured using a centred moving window, 5 nm s^{-1} in width. Colour scale as in **a**.

becomes apparent only as the amplitude rises. This association makes sense, because higher amplitudes (larger magnitude LFEs) suggest that the arresting mechanism is less strong such that slip can accelerate to higher velocities and larger fault areas, which could allow greater spatial separation between subsequent LFE nucleations. Indeed, if this effect results primarily from higher permeability rather than lower dilation, the incremental dilation associated with faster slip velocities during larger LFEs may further enhance transient permeability in the slipping region.

Tremor migration patterns and fault zone complexity

The strong variations in LFE source pair correlations at a given source separation distance (Supplementary Fig. 1) may reflect multiple factors. One likely factor is the fault geometry. As with typical earthquakes, ruptures tend to propagate further (resulting in large-magnitude events) for large, geometrically simple faults. Complexities such as bends and step-overs tend to inhibit rupture[33]. Although the timescales are different, the same is probably true for tremor and creep events. Migration should be inhibited between sources connected by a geometrically complex fault zone, such as sources on different fault strands. Variations in fault frictional properties and permeability may also be important—as discussed above, the tremor generation process itself may be integral to sustained high-speed propagation.

In general, stronger correlations are observed among sources at similar depths. This may reflect anisotropy in geometrical complexity, friction and permeability resulting from accumulated slip. As discussed above, accumulated slip probably produces fault corrugations aligned in the slip direction. Slip would also tend to elongate geologic units (for example, containing serpentinite) along the fault, creating similarly elongated zones of similar frictional or fluid properties.

Intriguingly, the migration patterns lend support to the complexity suggested by the LFE family locations, which previously could have been interpreted as an artefact of location uncertainty. In particular, locations show six LFE families offset from the main cluster of LFEs at the downdip end (Fig. 5). Five of these families (at ~26–29 km depth) interact strongly with each other and are offset ~4 km from the main cluster of LFEs in the fault-perpendicular direction. One LFE family, at nearly 30 km depth, is completely isolated from the other sources and offset nearly 10 km in the fault-perpendicular direction. This spatially and temporally isolated source exhibits intriguing patterns in recurrence intervals, at times oscillating between ~3 and ~6 days (ref. 34).

These patterns present tantalizing clues to the structure of the plate boundary at depth, perhaps hinting at past subduction along the continental margin. The geometry is consistent with the hypothesis that the San Andreas Fault in central California soles into the top of the stalled Monterey Microplate, a remnant of the subducted Farallon Plate that was captured by the Pacific Plate[35–37]. If so, the offset LFE families may be generated by strike slip on the shallowly dipping interface between the stalled slab and the North American Plate. Alternatively, they might instead reflect multiple steeply dipping fault strands at depth (Fig. 5c). Nevertheless, the presence of a fossil slab and serpentinized mantle wedge[38] would provide an attractive link between this section of the San Andreas Fault and fluid-rich subduction zones, where most tremor has thus far been observed. In fact, the region of the fault suggested to be underlain by the fossil Monterey Microplate[35] corresponds well with the current extent of tremor observations along the San Andreas.

Implications for deep fault zone deformation

Tremor source interactions constrain aspects of source physics and fault structure not otherwise apparent. On the basis of the observed migration characteristics, I explore a conceptual model

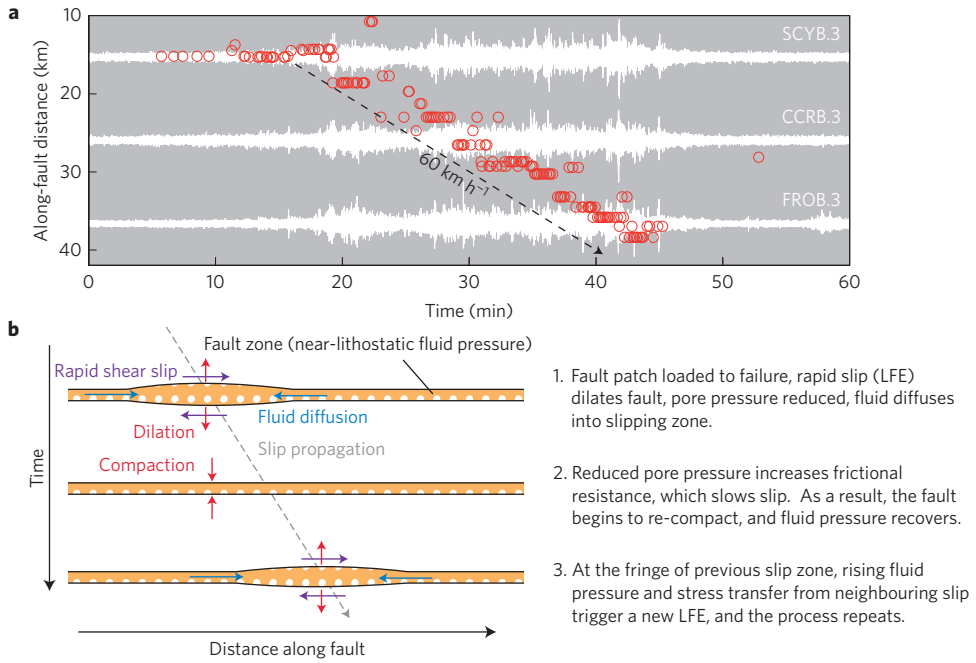

Figure 4 | Tremor propagation example and conceptual model. a, High-speed tremor propagation example. Red circles show LFE detections with location estimate of corresponding family. Corresponding tremor waveforms (ground velocity) recorded at three borehole seismometers (filtered 2–8 Hz, normalized) are shown in white. Dashed arrow shows velocity of 60 km h^{-1} for reference. Along-fault distance is referenced as in Fig. 1. Time is referenced to 16:15 UTC on 20 August 2004. **b**, Cartoon showing the proposed mechanism regulating high-speed tremor propagation. The feedback process of slip-induced dilatancy and its recovery may drive oscillating slip velocity and transient local fluid redistribution. The temporal scale of fluid diffusion may regulate the propagation speed. Bilateral propagation is sometimes also observed.

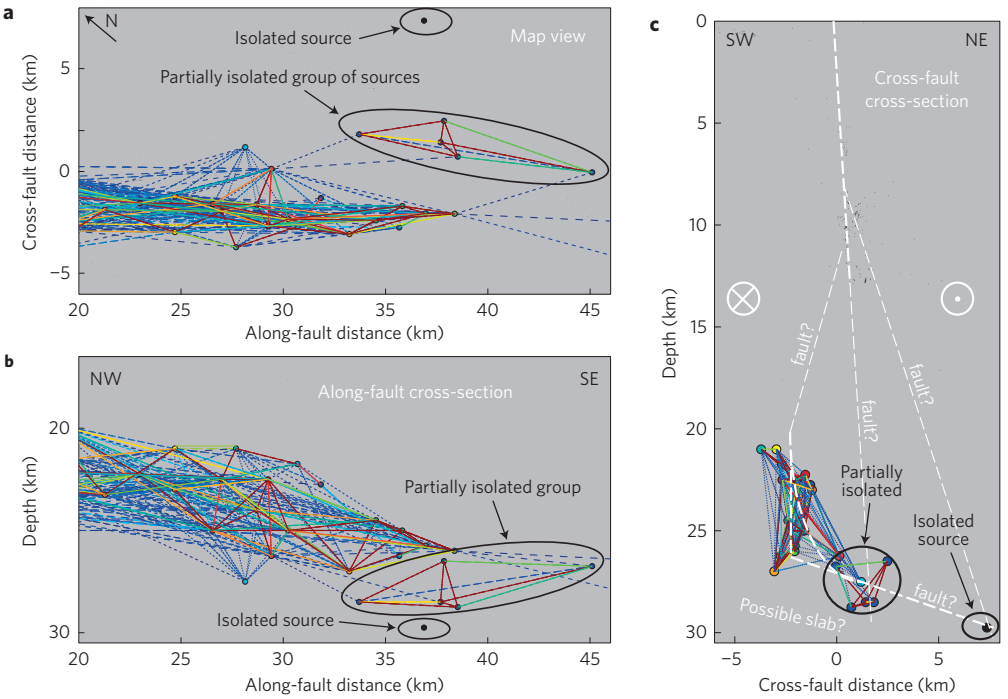

Figure 5 | LFE family locations and interactions suggest deep fault zone complexity, perhaps related to an underlying fossil slab. a, Zoomed map view (outlined area of Fig. 2a). **b**, Along-fault cross-section. **c**, Cross-fault cross-section. Symbols and colour scales are as in Fig. 2. The interaction patterns, in particular the partially isolated group of offset sources and the completely isolated source at greater offset (~10 km from main group), argue that the spread in locations is not simply an artefact of location errors. Plausible fault models include a multi-stranded fault or a nearly vertical fault soling into a shallowly dipping fault at the base of the crust (white dashed lines). The latter interpretation is consistent with recent stalled slab hypotheses[35,36].

of high-speed tremor propagation as a cascade of LFE ruptures regulated though a negative feedback process of slip-induced dilatancy. If so, then the LFE rupture process itself is important in dynamically maintaining this high-speed propagation, acting as a trigger to coherently release stress accumulated primarily by surrounding slow slip. Corroborating this hypothesis is the

observation that high-speed propagation is most extensive in areas of densely distributed, high-amplitude tremor sources, and absent across gaps in the tremor distribution (such as directly beneath Parkfield). This challenges the usual assumption that tremor is an entirely passive consequence of surrounding slow slip and suggests that high-speed tremor propagation is fundamentally distinct from slower $\sim$10 km d^{-1} propagation. Variations in permeability and fluid pressure may be important for explaining systematic variations in tremor amplitude, such as the large along-strike variations in tremor amplitude observed by ref. 15. Further numerical and laboratory work is needed to explore these effects more thoroughly.

Tremor migration patterns demonstrate pervasive heterogeneity within the deep fault zone, highlighting slip pathways and barriers. Among these features, the migration patterns imply that sources offset from the main trend are not simply artefacts of location uncertainty, but rather express actual complexity of the fault zone. In particular, LFE sources south of Parkfield that are offset up to 10 km northeast from the main trend perhaps hint at the presence of a fossil Farallon slab remnant at the base of the crust. If so, then the mantle San Andreas Fault zone may be deflected eastward along the slab surface, as some have proposed[35–37]. Future work should endeavour to constrain the sense of slip of these offset sources, which would further inform the configuration of the San Andreas beneath the crust.

Methods

I analyse tremor propagation using a catalogue of LFEs along the San Andreas Fault near Parkfield, California, derived as described by ref. 15. This catalogue, which begins in mid-2001 and is updated here to 6 November 2013, contains 850,149 LFEs. On the basis of the timing and shape of their waveforms, which reflects the source location, the catalogued LFEs are divided into 88 families with locations ranging $\sim$150 km along the fault and depths of 16–30 km, near the base of the crust (Fig. 1).

Identifying tremor migration episodes and measuring their orientation and velocity is simple in concept, yet can become complicated in practice. Starting from a catalogue of tremor locations with time, at least two general approaches can be considered: identify and characterize individual migration episodes[5,6,12]; or characterize migration behaviour of the catalogue as a whole, without criteria for individual episodes. Although the first option seems most intuitive, systematically discriminating individual tremor migration episodes requires several assumptions as to what exactly constitutes 'migration.' Perhaps because of this, most studies have identified tremor migration episodes at least in part by eye[5,6,13]. One of the few studies to examine tremor migration systematically used principle component analyses for tremor locations with time in multiple time window lengths, applying detection based on thresholds for linearity, angular distance and number of events[12]. In this work, I take a different approach—rather than identifying individual migration episodes, I examine cumulative interactions of tremor source pairs over the entire 12-year catalogue duration. To do this, I examine all possible pairs of source families (3,828 combinations), quantifying the temporal correlation between each pair. Each family includes events within a small but finite source region of the fault, with dimensions of perhaps $\sim$1 km, although sometimes larger[15].

To examine the interactions among family pairs, I formed a time series for each family representing the number of events during each minute. I then smoothed the time series over a running 3-min window. Finally, I cross-correlated the resulting smoothed time sequences for each possible family pair, measuring the normalized correlation coefficient at intervals of 1 min, with lags ranging from -120 to $+120$ min (see Fig. 1 inset). I used an empirically determined correlation threshold of 0.015 for links plotted in Fig. 2. This threshold choice was informed by the observed decay in correlation values as a function of interfamily distance (Supplementary Fig. 1). Although smoothing over multiple minutes helped achieve the most stable results, similar results were obtained without this smoothing. For family pairs correlating above the threshold, I estimated propagation velocities by the time lag of correlation peak and the estimated separation distance, with a minimum lag time of 2 min. To reliably measure velocity I additionally required that the peak correlation be at least twice the mean correlation over the examined lag range. Finally, I measured propagation asymmetry (tendency to propagate in one direction along the fault) by the comparing the integrated correlation function at positive and negative lag times (Fig. 1 inset), and calculating the excess fraction in a given direction along the fault (Fig. 2c). For example, the excess fraction in the southeast direction is $(N_{SE}-N_{NW})/(N_{SE}+N_{NW})$, where N_{SE} and N_{NW} are integrated correlation functions in the southeast and northwest directions, respectively (see Fig. 1 inset). I also measured the excess number of linked families that are northwest or southeast propagating (circle colours in Fig. 2c).

To observe family pair correlations and estimate propagation velocities, this method requires some level of consistency in the propagation velocities—it is in this way that high-speed migration between source pairs can be distinguished from a general association in time that arises for nearby sources that participate in the same multi-day tremor episodes. In practice, substantial variation in propagation velocity is observed, as reflected in the breadth of the correlation peaks, and is a major reason why maximum correlation coefficients typically remain low (see example in Fig. 1 inset).

For the comparison between LFE family amplitude and propagation velocity in Fig. 3c, I used the amplitude measure from ref. 15, which was calculated as the peak ground velocity for the 20th largest event for each family.

Received 23 June 2014; accepted 28 November 2014; published online 5 January 2015

References

1. Beroza, G. C. & Ide, S. Slow earthquakes and nonvolcanic tremor. *Annu. Rev. Earth Planet. Sci.* **39,** 271–296 (2011).
2. Shelly, D. R., Beroza, G. C. & Ide, S. Non-volcanic tremor and low frequency earthquake swarms. *Nature* **446,** 305–307 (2007).
3. Obara, K. Nonvolcanic deep tremor associated with subduction in southwest Japan. *Science* **296,** 1679–1681 (2002).
4. Dragert, H., Wang, K. & Rogers, G. Geodetic and seismic signatures of episodic tremor and slip in the northern Cascadia subduction zone. *Earth Planets Space* **56,** 1143–1150 (2004).
5. Shelly, D. R., Beroza, G. C. & Ide, S. Complex evolution of transient slip derived from precise tremor locations in western Shikoku, Japan. *Geochem. Geophys. Geosyst.* **8,** Q10014 (2007).
6. Ghosh, A. *et al.* Rapid, continuous streaking of tremor in Cascadia. *Geochem. Geophys. Geosyst.* **11,** Q12010 (2010).
7. Shelly, D. R. Migrating tremors illuminate complex deformation beneath the seismogenic San Andreas fault. *Nature* **463,** 648–652 (2010).
8. Houston, H., Delbridge, B. G., Wech, A. G. & Creager, K. C. Rapid tremor reversals in Cascadia generated by a weakened plate interface. *Nature Geosci.* **4,** 404–409 (2011).
9. Ando, R., Nakata, R. & Hori, T. A slip pulse model with fault heterogeneity for low-frequency earthquakes and tremor along plate interfaces. *Geophys. Res. Lett.* **37,** L10310 (2010).
10. Ando, R., Takeda, N. & Yamashita, T. Propagation dynamics of seismic and aseismic slip governed by fault heterogeneity and Newtonian rheology. *J. Geophys. Res.* **117,** B11308 (2012).
11. Rubin, A. M. Designer friction laws for bimodal slow slip propagation speeds. *Geochem. Geophys. Geosyst.* **12,** Q04007 (2011).
12. Obara, K., Matsuzawa, T., Tanaka, S. & Maeda, T. Depth-dependent mode of tremor migration beneath Kii Peninsula, Nankai subduction zone. *Geophys. Res. Lett.* **39,** L10308 (2012).
13. Ide, S. Striations, duration, migration and tidal response in deep tremor. *Nature* **466,** 356–359 (2010).
14. Nadeau, R. M. & Dolenc, D. Nonvolcanic tremors deep beneath the San Andreas Fault. *Science* **307,** 389 (2005).
15. Shelly, D. R. & Hardebeck, J. L. Precise tremor source locations and amplitude variations along the lower-crustal central San Andreas Fault. *Geophys. Res. Lett.* **37,** L14301 (2010).
16. Thomas, A. M., Bürgmann, R., Shelly, D. R., Beeler, N. M. & Rudolph, M. L. Tidal triggering of low frequency earthquakes near Parkfield, California: Implications for fault mechanics within the brittle-ductile transition. *J. Geophys. Res.* **117,** B05301 (2012).
17. Rubin, A. M. & Armbruster, J. G. Imaging slow slip fronts in Cascadia with high precision cross-station tremor locations. *Geochem. Geophys. Geosyst.* **14,** 5371–5392 (2013).
18. Kao, H., Wang, K., Dragert, H., Kao, J. Y. & Rogers, G. Estimating seismic moment magnitude (Mw) of tremor bursts in northern Cascadia: Implications for the "seismic efficiency" of episodic tremor and slip. *Geophys. Res. Lett.* **37,** L19306 (2010).
19. Samuelson, J., Elsworth, D. & Marone, C. Shear-induced dilatancy of fluid-saturated faults: Experiment and theory. *J. Geophys. Res.* **114,** B12404 (2009).
20. Segall, P., Rubin, A. M., Bradley, A. M. & Rice, J. R. Dilatant strengthening as a mechanism for slow slip events. *J. Geophys. Res.* **115,** B12305 (2010).
21. Yamashita, T. & Suzuki, T. Dynamic modeling of slow slip coupled with tremor. *J. Geophys. Res.* **116,** B05201 (2011).
22. Yamashita, T. Generation of slow slip coupled with tremor due to fluid flow along a fault. *Geophys. J. Int.* **193,** 375–393 (2013).

23. Segall, P. & Rice, J. R. Dilatancy, compaction, and slip instability of a fluid infiltrated fault. *J. Geophys. Res.* **100,** 22155–22171 (1995).
24. Shelly, D. R., Beroza, G. C., Ide, S. & Nakamula, S. Low-frequency earthquakes in Shikoku, Japan and their relationship to episodic tremor and slip. *Nature* **442,** 188–191 (2006).
25. Audet, P., Bostock, M. G., Christensen, N. I. & Peacock, S. M. Seismic evidence for overpressured subducted oceanic crust and megathrust fault sealing. *Nature* **457,** 76–78 (2009).
26. Thomas, A. M., Nadeau, R. M. & Burgmann, R. Tremor-tide correlations and near-lithostatic pore pressure on the deep San Andreas fault. *Nature* **462,** 1048–1051 (2009).
27. Beeler, N. M., Thomas, A., Bürgmann, R. & Shelly, D. Inferring fault rheology from low-frequency earthquakes on the San Andreas. *J. Geophys. Res.* **118,** 5976–5990 (2013).
28. Ghosh, A., Vidale, J. E., Sweet, J. R., Creager, K. C. & Wech, A. G. Tremor patches in Cascadia revealed by seismic array analysis. *Geophys. Res. Lett.* **36,** L17316 (2009).
29. Rice, J. R. in *Fault Mechanics and Transport Properties of Rocks* (eds Evans, B. & Wong, T-f.) 475–503 (Academic Press, 1992); http://go.nature.com/3Uia78
30. Ingebritsen, S. E. & Manning, C. E. Permeability of the continental crust: Dynamic variations inferred from seismicity and metamorphism. *Geofluids* **10,** 193–205 (2010).
31. Ingebritsen, S. E. & Manning, C. E. Geological implications of a permeability-depth curve for the continental crust. *Geology* **27,** 1107–1110 (1999).
32. Shelly, D. R. & Johnson, K. M. Tremor reveals stress shadowing, deep postseismic creep, and depth-dependent slip recurrence on the lower-crustal San Andreas fault near Parkfield. *Geophys. Res. Lett.* **38,** L13312 (2011).
33. Wesnousky, S. G. Predicting the endpoints of earthquake ruptures. *Nature* **444,** 358–360 (2006).
34. Shelly, D. R. Periodic, chaotic, and doubled recurrence intervals on the deep San Andreas Fault. *Science* **328,** 1385–1388 (2010).
35. Pikser, J. E., Forsyth, D. W. & Hirth, G. Along-strike translation of a fossil slab. *Earth Planet. Sci. Lett.* **331,** 315–321 (2012).
36. Wang, Y. *et al.* Fossil Slabs attached to unsubducted fragments of the Farallon Plate. *Proc. Natl Acad. Sci. USA* **110,** 5342–5346 (2013).
37. Bohannon, R. G. & Parsons, T. Tectonic implications of post-30 Ma Pacific and North American relative plate motions. *Geol. Soc. Am. Bull.* **107,** 937–959 (1995).
38. Kirby, S. H., Wang, K. & Brocher, T. M. A large mantle water source for the northern San Andreas fault system: A ghost of subduction past. *Earth Planets Space* **66,** 1–18 (2014).
39. Waldhauser, F. & Schaff, D. P. Large-scale relocation of two decades of Northern California seismicity using cross-correlation and double-difference methods. *J. Geophys. Res.* **113,** B08311 (2008).

Acknowledgements

I am very grateful for feedback and reviews from G. McLaskey, O. Kaven, D. Hill, J. Hardebeck, A. Thomas, D. Trugman and N. Beeler, all of which helped to improve the manuscript. The HRSN borehole seismic network, which was used to detect LFEs examined in this study, is operated by UC Berkeley. Data were obtained through the Northern California Earthquake Data Center (NCEDC).

Additional information

Supplementary information is available in the online version of the paper. Reprints and permissions information is available online at www.nature.com/reprints.

Competing financial interests

The author declares no competing financial interests.